

Interpretation of the energy spectrum observed with the Telescope Array detectors

Eiji Kido* for the Telescope Array Collaboration

Institute for Cosmic Ray Research, University of Tokyo, 5-1-5 Kashiwanoha, Chiba 277-8582, Japan

E-mail: ekido@icrr.u-tokyo.ac.jp

The energy spectrum of cosmic rays above $10^{18.2}$ eV is analyzed using Telescope Array (TA) surface detectors (SDs). The energy spectrum of cosmic rays above $10^{17.2}$ eV is analyzed using TA fluorescence detector (TAFD) monocular mode. In this paper, the break point of the energy spectrum at around $10^{18.7}$ eV which is known as “ankle” region is discussed using the data. We explored the possibility that cosmic ray protons from extra galactic sources can explain the feature of the spectrum shape in the ankle region. Magnetic fields in intergalactic space are also considered to discuss especially the low energy part of the data.

*35th International Cosmic Ray Conference — ICRC2017
10–20 July, 2017
Bexco, Busan, Korea*

*Speaker.

1. Introduction

The Telescope Array (TA) [1] is the largest cosmic-ray observatory in the Northern Hemisphere. The TA experiment has 507 surface particle detectors (SDs) on a square grid with 1.2 km spacing covering approximately 700 km². The SDs are surrounded by three fluorescence detector (FD) stations (12, 12 and 14 telescopes). The duty cycle of the SD array is greater than 95% throughout 5-year observation period, whereas the FD duty cycle is about 10% because the data are taken only on moonless clear nights. The measurement of the energy spectrum using the TA SD data for four years was published in Ref. [2]. The energy spectrum was updated using the TA SD data for the seven years between 2008 May 11 and 2015 May 11 [3]. This energy spectrum shows the ankle at around 10^{18.7} eV and the cutoff at around 10^{19.8} eV. The energy spectrum observed with the monocular mode of TA FD for seven years was published in Ref. [4]. This energy spectrum covers a broad energy range above 10^{17.2} eV.

The interpretation of cosmic ray spectrum features crucially depends on assumptions about the UHECR composition. In particular the suppression of UHECR flux above around 10^{19.8} eV is expected for protons due to GZK mechanism [5, 6] while in the case of heavy nuclei as primaries this feature may signal the natural cutoff in the maximal acceleration energy of sources. As it was pointed out in Ref. [7] this model applied to HiRes data can explain both "ankle" and cut-off features of the spectrum as a result of e^+e^- -pair production and pion production on the cosmic microwave background (CMB) without introducing any extra components or fine tuning the maximal source acceleration energy.

As shown in Ref. [8] and Ref. [9], the implication of the different cutoff energies in different sky area is obtained in TA SD energy spectrum. In this paper, we attempt to fit the energy spectrum at only around the ankle region measured by the TA SD and the monocular mode of TA FD with the pure proton source model to discuss the general feature of the energy spectrum.

In the next section, the model calculations and the fitting procedure are explained, and the fitted results are shown in section 3 and 4. The conclusions and discussions are shown in section 5.

2. Methodology

The factors which define the observed cosmic ray spectrum can be divided in two groups:

- properties of sources i.e. distribution of sources in power, spectrum and maximal energy
- properties of the media i.e. photon backgrounds, magnetic fields and their evolution

Like in many previous works in this paper we attempt to fit the experimental data using simple phenomenological model for the source spectrum and evolution:

$$Q(E, z) = \alpha E^{-p} (1+z)^{3+m}, \quad E < E_{\max}, z < z_{\max}, \quad (2.1)$$

where α , p , m , E_{\max} and z_{\max} are free parameters. The parameter m parameterizes the evolution of the source density per comoving volume. $m = 0$ if the source density is constant per comoving volume. The effect of sources located at $z > 0.7$ and $z > 1.5$ is negligible for cosmic ray energies $E > 10^{18.2}$ eV and $E > 10^{17.5}$ eV respectively. The energy threshold E_{th} between 10^{17.5} eV and

$10^{18.2}$ eV is discussed in this paper. The parameter E_{\max} in practice has small effect on fit goodness if $E_{\max} < 2 \times 10^{20}$ eV. Throughout this paper we use fixed values of $E_{\max} = 10^{21}$ eV and $z_{\max} = 2$ unless explicitly stated. To concentrate on the discussion of the ankle region, only the data points below $E < 10^{19}$ eV are used for the comparison with this model.

The main attenuation mechanism for UHECR protons is photopion production and e^+e^- -pair production on the cosmic microwave background (CMB). However, interactions with infrared (and optic) background component (IRB) and deflections by the intergalactic magnetic field (IGMF) could lead to extra attenuation. The last two factors are currently poorly known. The existing model calculations of the IRB spectral density [10, 11, 12] may differ by factor of 2 at redshift $z = 0$ and moreover the uncertainty grows with redshift. The effect of IGMF was simulated following the procedure in Ref. [13, 14].

Finally, to consider systematic uncertainty in the measurement of cosmic ray energies we introduce shift of experimental energy scale as an additional free parameter $\Delta \log E = \log E - \log E_{\text{obs}}$. Here and below E_{obs} is the measured energy and the base of the logarithm is 10.

2.1 Simulation of the propagation of protons

We use publicly available numerical code [15] to simulate the attenuation of protons. This code was developed in Ref. [16]. The code calculates the average propagated energy spectrum by solving 1D transport equation assuming rectilinear propagation of cosmic rays. The above code takes into account e^+e^- pair production process using continuous energy loss approximation, which is very precise for frequent interactions with small energy loss in a single interaction. For the pion production, the code utilizes the interaction rates derived with SOPHIA code [17]. The code contains several implementations of IRB models. Unless otherwise stated below we use the Kneiske et. al. best-fit model [11] for IRB. We also employ CRPropa v2.0.3 propagation code [18] to estimate the systematic uncertainties of spectrum fitting.

To consider the effect of IGMF, the assumption of rectilinear propagation of cosmic rays cannot be used. Another calculation code was made to consider IGMF and the simulation results are shown in section 4. The interpolation between rectilinear and diffusive regimes is calculated here. In this simulation, simplified magnetic fields with no structure are assumed. The lattice distribution of sources with distance between sources $d = 10$ Mpc is assumed. The coherent magnetic field B_c based on 1 Mpc basic scale of turbulence is taken as a free parameter. IRB models are not implemented in this code yet.

2.2 Model fitting of the data

To concentrate on the discussion of the ankle region, only the data points below $E < 10^{19}$ eV are used for the model fitting. We employ a binned likelihood analysis method with likelihood function of Gaussian distribution. We conservatively estimate the total flux determination uncertainties as $\sigma_{\text{TOT}} = \sqrt{\sigma_{\text{STAT}}^2 + \sigma_{\text{SYS}}^2}$, where $\sqrt{N_i}$ is the statistical error of the observed number of events N_i in each energy bin and σ_{SYS} is the systematic uncertainty of the flux. As mentioned above we consider the systematic uncertainty of energy determination in the experiment by introducing the energy shift as a free parameter in the range $-0.11 \leq \Delta \log E \leq 0.09$, because the systematic uncertainty of the energy determination is estimated to be 21% [3]. We combined the fit result of TA

SD data with the fit result of TA FD monocular data by simply combining the logarithms of their likelihood values. TA FD monocular data above $10^{18.2}$ eV is removed from this combining process because many events are also used in TA SD data. The degrees of freedom of the likelihood equal to number of energy bins minus number of fitting parameters. In this case, number of fitting parameters is 4. The best-fit parameters are determined by maximizing the likelihood L . We determine the confidence region of each free parameter using $\Delta(\ln L) = (\ln L_{\max}) - (\ln L)$, where L_{\max} is the maximum value of likelihood L .

3. Fit results

We show the expected energy spectrum with source parameters determined by fitting the TA energy spectrum above $E_{th} = 10^{17.5}$ eV in Fig. 1. The fit parameters are determined such as $p = 2.34^{+0.13}_{-0.05}$, $m = 4.1^{+0.4}_{-0.8}$ and $\Delta \log E = -0.11^{+0.11}_{-0.00}$ when $E_{th} = 10^{17.5}$ eV. $(-2 \ln L_{\max})/\text{d.o.f.} = 5.4/11$ is obtained. The similar fitting parameters are obtained if $E_{th} < 10^{18}$ eV. The determined fit parameters p and m are shown in Fig. 2 and Fig. 3 when $E_{th} = 10^{17.5, 17.6, \dots, 18.2}$ eV.

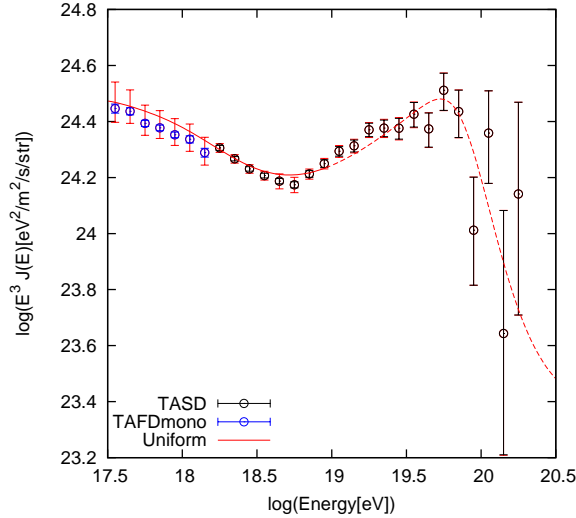


Figure 1: The black data points denote the energy spectrum measured by TA SD and the statistical errors. The blue data points denote the energy spectrum measured by the monocular mode of TA FD and the statistical errors. The red error bars denote overall uncertainty including the statistical errors and the systematic errors. The red solid and broken lines denote the best fit expected energy spectrum with $p = 2.34$, $m = 4.1$, $\Delta \log E = -0.11$ to all the data points above $10^{17.5}$ eV and below 10^{19} eV. $(-2 \ln L)/\text{d.o.f.}$ is $5.4/11$. The red broken line is not used for the fitting. In this figure, the energy scale of the data points is fixed and the energy scale of the model is shifted.

4. Fit results considering the effect of IGMF

Fig.4 shows the simulated energy spectrum with different B_c values when $p = 2.34$, $m = 4.1$ and $\Delta \log E = -0.11$. In case of large m , the diffused fluxes of distant sources especially make a steep low energy cutoff of the energy spectrum. We found that the condition $B_c = 0.01$ nG produce the decrease of the proton fraction between $10^{17.5}$ eV and 10^{18} eV as shown in Fig.5.

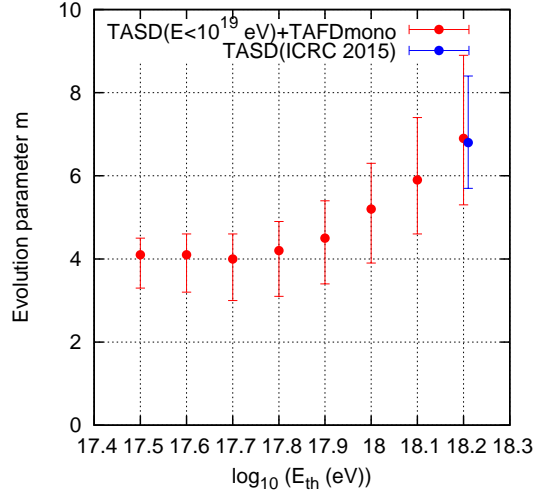


Figure 2: The red points denote the determined fitting parameter m when different lower limits E_{th} of the data are used for fitting. The data with $E > 10^{19}$ eV is not used for fitting to obtain red points. The blue point is the determined parameter which was obtained using all the TASD data points above $10^{18.2}$ eV [19].

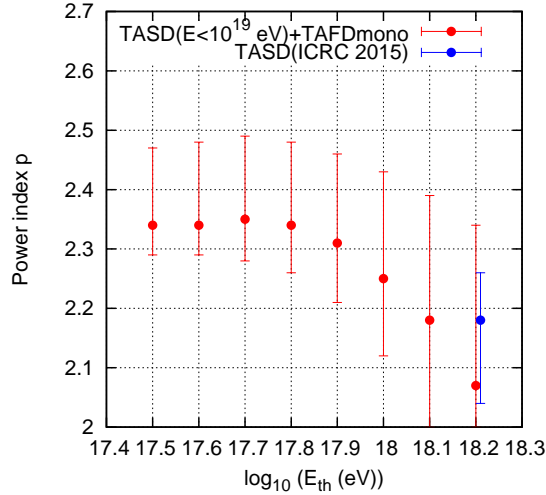


Figure 3: The red points denote the determined fitting parameter p when different lower limits E_{th} of the data are used for fitting. The data with $E > 10^{19}$ eV is not used for fitting to obtain red points. The blue point is the determined parameter which was obtained using all the TASD data points above $10^{18.2}$ eV [19].

5. Conclusions and discussion

The data points around the ankle region is successfully fitted with pure proton model from the point of the shape of the energy spectrum. The fit parameters $p = 2.34^{+0.13}_{-0.05}$, $m = 4.1^{+0.4}_{-0.8}$ and $\Delta \log E = -0.11^{+0.11}_{-0.00}$ are obtained when all of the data points above $E_{th} = 10^{17.5}$ eV are used for the fitting. We found that the condition $B_c = 0.01$ nG can produce the cutoff of the proton fraction between $10^{17.5}$ eV and 10^{18} eV with the best-fit model parameters $p = 2.34$, $m = 4.1$ and $\Delta \log E = -0.11$. Composition measurements by HiRes-MIA [20] and Auger [21] indicate that the

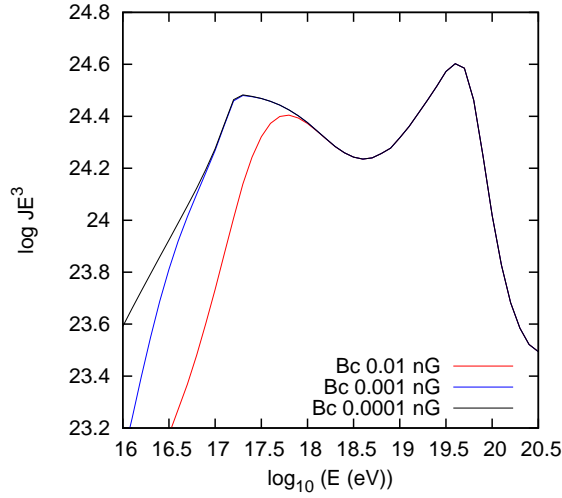


Figure 4: The simulated energy spectra with $B_c = 0.0001$ nG, 0.001 nG, 0.01 nG when $p = 2.35$, $m = 4.1$ and $\Delta \log E = -0.11$. Bohm diffusion $D(E) \propto E$ is assumed. The lattice distribution of sources with distance between sources $d = 10$ Mpc is assumed.

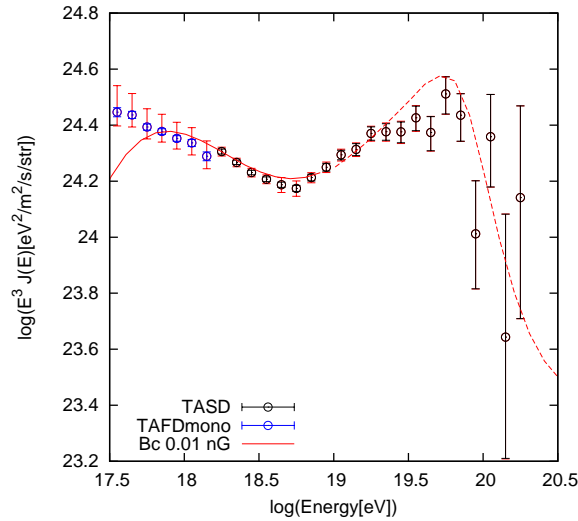


Figure 5: The same data points as in Fig. 1 are shown. The red solid and broken lines denote the simulated energy spectrum with $B_c = 0.01$ nG using best-fit parameters $p = 2.35$, $m = 4.1$ and $\Delta \log E = -0.11$ obtained in Fig. 1. In this figure, the energy scale of the data points is fixed and the energy scale of the model is shifted. IRB models are not implemented yet in this figure. The difference of IRB leads to the shape of the simulated energy spectrum between Fig. 1 and this figure at around $10^{19.5}$ eV.

composition below 10^{18} eV is not pure protons, hence the proton model, indicated by the red line in Fig. 5, should be below the data points. A lower value of m also produces this effect.

6. Acknowledgements

The Telescope Array experiment is supported by the Japan Society for the Promotion of Science through Grants-in-Aids for Scientific Research on Specially Promoted Research (15H05693) and for Scientific Research (S) (15H05741), and the Inter-University Research Program of the Institute for Cosmic Ray Research; by the U.S. National Science Foundation awards PHY-0307098, PHY-0601915, PHY-0649681, PHY-0703893, PHY-0758342, PHY-0848320, PHY-1069280, PHY-1069286, PHY-1404495 and PHY-1404502; by the National Research Foundation of Korea (2015R1A2A1A01006870, 2015R1A2A1A15055344, 2016R1A5A1013277, 2007-0093860, 2016R1A2B4014967); by the Russian Academy of Sciences, RFBR grant 16-02-00962a (INR), IISN project No. 4.4502.13, and Belgian Science Policy under IUAP VII/37 (ULB). The foundations of Dr. Ezekiel R. and Edna Wattis Dumke, Willard L. Eccles, and George S. and Dolores Doré Eccles all helped with generous donations. The State of Utah supported the project through its Economic Development Board, and the University of Utah through the Office of the Vice President for Research. The experimental site became available through the cooperation of the Utah School and Institutional Trust Lands Administration (SITLA), U.S. Bureau of Land Management (BLM), and the U.S. Air Force. We appreciate the assistance of the State of Utah and Fillmore offices of the BLM in crafting the Plan of Development for the site. We also wish to thank the people and the officials of Millard County, Utah for their steadfast and warm support. We gratefully acknowledge the contributions from the technical staffs of our home institutions. An allocation of computer time from the Center for High Performance Computing at the University of Utah is gratefully acknowledged.

References

- [1] <http://www.telescopearray.org/>
- [2] T. Abu-Zayyad et al., *ApJ*. **768** L1 (2013).
- [3] D. Ivanov et al., *PoS(ICRC2015)*349 (2015).
- [4] R.U. Abbasi et al., *Astropart. Phys.* **80**, 131 (2016).
- [5] K. Greisen, *Phys. Rev. Lett.* **16**, 748 (1966).
- [6] G.T. Zatsepin and V.A. Kuz'min, *J. Exp. Theor. Phys. Lett.* **4**, 78 (1966).
- [7] V.S. Berezinsky, A. Gazizov, & S. Grigorieva, *Phys. Rev. D* **74**, 043005 (2006).
- [8] T. Nonaka for the Telescope Array Collaboration, 35th ICRC (Busan), CRI207 (2017).
- [9] D. Ivanov et al., *PoS(ICRC2017)*496 (2017).
- [10] A. Franceschini, G. Rodighiero and M. Vaccari, *Astron. Astrophys.* **487**, 837 (2008) [arXiv:0805.1841 [astro-ph]]. F. W. Stecker, M. A. Malkan and S. T. Scully, *Astrophys. J.* **761**, 128 (2012). S. T. Scully, M. A. Malkan and F. W. Stecker, [arXiv:1401.4435 [astro-ph.HE]]. J. R. Primack, R. C. Gilmore and R. S. Somerville, *AIP Conf. Proc.* **1085**, 71 (2009); J. D. Finke, S. Razzaque and

- C. D. Dermer, *Astrophys. J.* **712**, 238 (2010). Y. Inoue, S. Inoue, M. A. R. Kobayashi, R. Makiya, Y. Niino and T. Totani, *Astrophys. J.* **768**, 197 (2013) [arXiv:1212.1683 [astro-ph.CO]].
- [11] T. M. Kneiske et al., *Astron. Astrophys.* **386**(2002) 1; *ibid.*, **413** (2004) 807.
- [12] T. M. Kneiske and H. Dole, [arXiv:1001.2132 [astro-ph.CO]].
- [13] V. Berezhinsky and A. Z. Gazizov, *Astrophys. J.* **643**, 8 (2006).
- [14] R. Aloisio, V. Berezhinsky and A. Z. Gazizov, *Astrophys. J.* **693**, 1275 (2009).
- [15] O. E. Kalashev and E. Kido, *JETP*, **120**, 5, 790 (2015)
- [16] O.E. Kalashev, PhD thesis, INR RAS, Moscow 2003. G.B. Gelmini, O. Kalashev and D. V. Semikoz, *JCAP* **1201**, 044 (2012) [arXiv:1107.1672 [astro-ph.CO]]. K. Arisaka, G.B. Gelmini, M.D. Healy, O. E. Kalashev and J. Lee, *JCAP* **0712**, 002 (2007) [arXiv:0709.3390 [astro-ph]].
- [17] A. Mucke, R. Engel, J. P. Rachen, R.J. Protheroe, T. Stanev, *Computer Physics Communications* **124** 290-314 (2000).
- [18] K. -H. Kampert, J. Kulbartz, L. Maccione, N. Nierstenhoefer, P. Schiffer, G. Sigl and A. R. van Vliet, *Astropart. Phys.* **42**, 41 (2013) [arXiv:1206.3132 [astro-ph.IM]].
- [19] E. Kido and O.E. Kalashev et al., *PoS(ICRC2015)*258 (2015).
- [20] R.U. Abbasi et al. HiRes Collaboration, *Phys. Rev. Lett.* **104**, 161101 (2010).
- [21] A. Aab et al. Pierre Auger Collaboration, *Phys. Rev. D.* **90**, 122006 (2014).